

## Article

# Generalized Asymmetric Hermite–Gaussian and Laguerre–Gaussian Beams

Eugeny G. Abramochkin <sup>1</sup>, Victor V. Kotlyar <sup>2,3</sup>, Alexey A. Kovalev <sup>2,3,\*</sup> and Sergey S. Stafeev <sup>2,3</sup><sup>1</sup> Lebedev Physical Institute, 221 Novo-Sadovaya St., 443034 Samara, Russia; ega@fian.smr.ru<sup>2</sup> Image Processing Systems Institute of the RAS—Branch of FSRC “Crystallography & Photonics” of the RAS, 151 Molodogvardeyskaya St., 443001 Samara, Russia; kotlyar@ipsiras.ru (V.V.K.); stafeev@ipsiras.ru (S.S.S.)<sup>3</sup> Samara National Research University, 34 Moskovskoe Shosse, 443086 Samara, Russia

\* Correspondence: alanko@ipsiras.ru

**Abstract:** We derive analytical formulae for the complex amplitudes of variants of generalized Hermite–Gaussian (HG) and Laguerre–Gaussian (LG) beams. We reveal that, at particular values of parameters of the exact solution of the paraxial propagation equation, these generalized beams are converted into conventional elegant HG and LG beams. We also deduce variants of asymmetric HG and LG beams that are described by complex amplitudes in the form of Hermite and Laguerre polynomials whose argument is shifted into the complex plane. The asymmetric HG and LG beams are, respectively, shown to present the finite superposition of the generalized HG and LG beams. We also derive an explicit relationship for the complex amplitude of a generalized vortex HG beam, which is built as the finite superposition of generalized HG beams with phase shifts. Newly introduced asymmetric HG and LG beams show promise for the study of the propagation of beams carrying an orbital angular momentum through the turbulent atmosphere. One may reasonably believe that the asymmetric laser beams are more stable against turbulence when compared with the radially symmetric ones.

**Keywords:** asymmetric beam; Hermite–Gaussian beam; Laguerre–Gaussian beam; free space propagation



**Citation:** Abramochkin, E.G.; Kotlyar, V.V.; Kovalev, A.A.; Stafeev, S.S. Generalized Asymmetric Hermite–Gaussian and Laguerre–Gaussian Beams. *Photonics* **2023**, *10*, 606. <https://doi.org/10.3390/photonics10060606>

Received: 24 April 2023

Revised: 17 May 2023

Accepted: 19 May 2023

Published: 23 May 2023



**Copyright:** © 2023 by the authors. Licensee MDPI, Basel, Switzerland. This article is an open access article distributed under the terms and conditions of the Creative Commons Attribution (CC BY) license (<https://creativecommons.org/licenses/by/4.0/>).

## 1. Introduction

Laser beams whose complex amplitudes can be described by explicit formulae as exact solutions of the paraxial propagation equation have invariably been the focus of attention of optical researchers. The fact is that knowledge of the complex amplitude of the beams at any distance from the source plane enables the full set of their parameters to be predicted, including the intensity distribution, intensity moments, total power of the beam, topological charge, orbital angular momentum, and beam divergence. Propagating in free space, such beams are usually either structurally stable (conserving their intensity pattern up to a scale and rotation) or change weakly, with their complex amplitude expressed by an elegant mathematical relationship. While such beams are abundant, two of the most familiar are standard Hermite–Gaussian (HG) and Laguerre–Gaussian (LG) laser beams. For the first time, HG beams were discussed in Ref. [1] and elegant HG (eHG) beams were studied in Ref. [2]. Various kinds of generalized HG (gHG) beams have also been investigated [3–7]. More specifically, in Ref. [3], the generalized HG beams were defined as conventional HG beams with a parameter, whereas in Ref. [7], the generalized beams were obtained as the superposition of conventional HG beams propagating with the same phase velocity. The parameter of the generalized HG beams is in the argument of the Hermite polynomials and defines the ratio between the widths of the Gaussian envelope and of the Hermite polynomials. At a certain value of this parameter, the generalized HG beam reduces to the conventional HG beam. Combined parametric Hermite–Laguerre–Gaussian beams, introduced in Ref. [8], were shown to transform into standard HG beams or LG beams

depending on the specific value of the parameter. A relationship between the HG and LG beams was established in Ref. [9], and vortex HG beams constructed as the superposition of conventional HG beams with phase shifts were studied in Ref. [10]. For the first time, the standard LG beams were analyzed as laser cavity modes in Ref. [1] before being shown to propagate in an ABCD system [11]. Issues relating to the study of LG modes include their transformation and focusing with the aid of an axicon [12,13] and their representation through Wigner distribution functions [14]. Non-paraxial variants of the HG and LG beams have also been analyzed [15], as well as studying double-frequency LG beams and their transformation into conventional LG beams [16]. Other types of beams have been studied, including asymmetric LG beams [17] and the laser-aided intra-cavity shaping of asymmetric HG beams [18], which were then transformed into asymmetric LG beams using a mode converter [9]. A technique for generating vector laser beams with the aid of LG beams has been proposed [19]. The generation of LG beams in a wide frequency band by second harmonic generation has been reported [20], whereas conventional LG beams can be realized using a standard spatial light modulator (SLM) [21].

LG and HG beams with different modifications have wide practical applications. For instance, in works [22,23], structurally stable beams are considered which are coaxial superpositions of a finite number of the conventional HG beams with complex coefficients–parameters. The authors demonstrated that changing these parameters leads to oscillations of the orbital angular momentum of such a superposition and that it can achieve large positive and negative values. Using different methods, the LG beams can be converted into HG beams. In ref. [9], using a mode converter composed of two cylindrical lenses, the HG beams were, for the first time, converted to the LG beams. Such transformation can also be performed by tilting a diffractive optical element [24]. The LG beam generated this way is elliptic. Using an elliptically squeezed axicon, a Bessel–Gaussian beam can be transformed to an HG beam, which allows us to determine the topological charge of the optical vortex [25]. Besides the asymmetric LG and HG beams, asymmetric Bessel beams [26] and Bessel–Gaussian beams [27] are known, which are also used for manipulating microparticles [28]. Ref. [20] contains a survey of works on the subject of generating the LG beams. The survey lists passive and active methods for generating the LG beams. Passive methods include cylindrical lens mode converters [29], spiral zone plates [30], fork-shaped grating [31], non-spiral phase plate [32] and q-plate [33]. Active methods for LG beams generation include addition into a laser resonator such elements as plano-convex lens [34,35], point defect spatial filter [36], special resonant cavity mirrors such as SLM [37,38] and spot-defect mirror [39–43].

In this work, we discuss variants of generalized HG and LG beams, using which we generate asymmetric gHG and gLG beams, with the former obtained in two different variants. Asymmetric Bessel–Gaussian and LG beams have been known to show high stability upon propagation in a turbulent medium [44,45], prompting the exploration of other types of asymmetric HG and LG beams as promising candidates for monitoring the atmospheric turbulences.

## 2. Generalized Hermite–Gaussian and Laguerre–Gaussian Beams

It is well known that the complex amplitudes of standard HG and LG beams are as follows:

$$HG_{n,m}(x, y, z) = \frac{1}{|q|} \exp\left(-\frac{x^2 + y^2}{w_0^2 q} - i(n + m + 1)\arg q\right) H_n\left(\frac{\sqrt{2}x}{w_0|q|}\right) H_m\left(\frac{\sqrt{2}y}{w_0|q|}\right), \quad (1)$$

$$LG_{n,\pm m}(r, \varphi, z) = \frac{1}{|q|} \exp\left(-\frac{r^2}{w_0^2 q} - i(2n + m + 1)\arg q\right) \left(\frac{re^{\pm i\varphi}}{w_0|q|}\right)^m L_n^m\left(\frac{2r^2}{w_0^2|q|^2}\right). \quad (2)$$

Here,  $(x, y, z)$  and  $(r, \varphi, z)$  are Cartesian and cylindrical coordinates;  $q = q(z) = 1 + iz/z_0$  is an auxiliary complex parameter;  $z_0 = \pi w_0^2/\lambda$  is the Rayleigh range;  $\lambda$  is the wavelength;  $w_0$  is the waist radius of the Gaussian beam,  $n, m$  are nonnegative integers;  $w(z) = w_0|q|$

is the beam radius at distance  $z$  from the waist,  $\gamma(z) = \arg q = \arctan(z/z_0)$  is the Gouy phase;  $H_m(\cdot)$  and  $L_n^m(\cdot)$  are Hermite and Laguerre polynomials.

An elegant form of the HG and LG beams can be written as

$$\text{eHG}_{n,m}(x, y, z) = \frac{1}{q^{(n+m+2)/2}} \exp\left(-\frac{x^2 + y^2}{w_0^2 q}\right) H_n\left(\frac{x}{w_0 \sqrt{q}}\right) H_m\left(\frac{y}{w_0 \sqrt{q}}\right), \quad (3)$$

$$\text{eLG}_{n,\pm m}(r, \varphi, z) = \frac{1}{q^{n+1}} \exp\left(-\frac{r^2}{w_0^2 q}\right) \left(\frac{r e^{\pm i\varphi}}{w_0 q}\right)^m L_n^m\left(\frac{r^2}{w_0^2 q}\right). \quad (4)$$

Generalized versions of HG and LG beams are as follows [5]:

$$\begin{aligned} \text{gHG}_{n,m}(x, y, z|a, b) &= \frac{1}{q} \exp\left(-\frac{x^2 + y^2}{w_0^2 q}\right) \left(\frac{1-aq}{q}\right)^{n/2} \left(\frac{1-bq}{q}\right)^{m/2} \\ &\times H_n\left(\frac{x}{w_0 \sqrt{q(1-aq)}}\right) H_m\left(\frac{y}{w_0 \sqrt{q(1-bq)}}\right), \end{aligned} \quad (5)$$

$$\text{gLG}_{n,\pm m}(r, \varphi, z|a) = \frac{1}{q} \exp\left(-\frac{r^2}{w_0^2 q}\right) \left(\frac{1-aq}{q}\right)^n \left(\frac{r e^{\pm i\varphi}}{w_0 q}\right)^m L_n^m\left(\frac{r^2}{w_0^2 q(1-aq)}\right). \quad (6)$$

In Equations (5) and (6),  $a$  and  $b$  are dimensionless parameters. Here, and in the following text, we use a vertical line to separate variables and parameters.

When  $a = b = 0$ , these beams are reduced to eHG and eLG beams, while for  $a = b = \frac{1}{2}$ , we obtain standard HG beams,  $2^{(n+m)/2} \text{gHG}_{n,m}(x, y, z|\frac{1}{2}, \frac{1}{2}) = \text{HG}_{n,m}(x, y, z)$ , and LG beams,  $2^n \text{gLG}_{n,\pm m}(x, y, z|\frac{1}{2}) = \text{LG}_{n,\pm m}(x, y, z)$ . Other forms of generalized Gaussian beams can also be found [6,7].

### 3. Asymmetric Generalized Hermite–Gaussian and Laguerre–Gaussian Beams

Asymmetric LG beams obtained by shifting the argument of the complex amplitude function into the complex domain have previously been reported [17]. Laser-generated asymmetric LG beams that were then converted into asymmetric LG modes using a mode converter [9] have been realized [18]. The asymmetric LG modes have been used to steer microparticles along an arc [46], as well as for non-invasively capturing and moving biological microobjects [28]. We note that it is also possible to realize asymmetric HG beams from asymmetric LG beams using a mode converter [9]. In this work, we demonstrate that asymmetric HG and LG beams are composed of a finite set of gHG and gLG beams. Actually, arguments of Hermite and Laguerre polynomials can be shifted using the following well-known sums [47,48]:

$$\begin{aligned} \sum_{k=0}^n \binom{n}{k} (2t)^{n-k} H_k(x) &= H_n(x+t), \\ \sum_{k=0}^n \frac{t^k}{k!} L_{n-k}^{m+k}(x) &= L_n^m(x-t). \end{aligned} \quad (7)$$

Making use of the sums in (7), the following relationships for complex amplitudes of gLG and gHG beams can be shown to hold:

$$\begin{aligned} \sum_{k=0}^n \frac{t^k}{k!} \text{gLG}_{n-k,m+k}(r, \varphi, z|a) &= \frac{1}{q} \exp\left(-\frac{r^2}{w_0^2 q}\right) \\ &\times \sum_{k=0}^n \frac{t^k}{k!} \left(\frac{1-aq}{q}\right)^{n-k} \left(\frac{r e^{i\varphi}}{w_0 q}\right)^{m+k} L_{n-k}^{m+k}\left(\frac{r^2}{w_0^2 q(1-aq)}\right) \\ &= \frac{1}{q} \exp\left(-\frac{r^2}{w_0^2 q}\right) \left(\frac{1-aq}{q}\right)^n \left(\frac{r e^{i\varphi}}{w_0 q}\right)^m L_n^m\left(\frac{r^2 - tq w_0 r e^{i\varphi}}{w_0^2 q(1-aq)}\right) = \text{gLG}_{n,m}(r, \varphi, z|a, t). \end{aligned} \quad (8)$$

$$\begin{aligned}
 & \sum_{\nu=0}^n \sum_{\mu=0}^m \binom{n}{\nu} \binom{m}{\mu} (2\tau)^{n-\nu} (2t)^{m-\mu} \text{gHG}_{\nu,\mu}(x, y, z|a, b) \\
 &= \frac{1}{q} \exp\left(-\frac{x^2+y^2}{w_0^2 q}\right) \sum_{\nu=0}^n \binom{n}{\nu} (2\tau)^{n-\nu} \left(\frac{1-aq}{q}\right)^{\nu/2} H_{\nu}\left(\frac{x}{w_0\sqrt{q(1-aq)}}\right) \\
 &\times \sum_{\mu=0}^m \binom{m}{\mu} (2t)^{m-\mu} \left(\frac{1-bq}{q}\right)^{\mu/2} H_{\mu}\left(\frac{y}{w_0\sqrt{q(1-bq)}}\right) \\
 &= \frac{1}{q} \exp\left(-\frac{x^2+y^2}{w_0^2 q}\right) \left(\frac{1-aq}{q}\right)^{n/2} \left(\frac{1-bq}{q}\right)^{m/2} H_n\left(\frac{x+\tau w_0 q}{w_0\sqrt{q(1-aq)}}\right) H_m\left(\frac{y+t w_0 q}{w_0\sqrt{q(1-bq)}}\right) \\
 &= \text{gHG}_{n,m}(x, y, z|a, b, \tau, t).
 \end{aligned} \tag{9}$$

In (8), the parameter  $a$  defines the ratio of the widths of the Gaussian function and Laguerre polynomial, whereas the complex parameter  $t$  defines the degree of LG beam asymmetry. Actually, it is the absolute value of  $t$  that affects the asymmetry. As seen in Equation (8), the argument of  $t$  only rotates the transverse pattern by the angle of  $\arg t$  (clockwise if  $\arg t > 0$  and counterclockwise if  $\arg t < 0$ ). In a similar way, in (9), the parameters  $a$  and  $b$  define the relative width of the Hermite polynomial along the  $x$ - and  $y$ -axes compared to the Gaussian function width, whereas the complex parameters  $\tau$  and  $t$  define the degree of HG beam asymmetry along the  $x$ - and  $y$ -axes. We note that the asymmetric LG beam in (8) is different from the similar asymmetric beam discussed in Ref. [18] because, in the latter case, the argument was shifted into the complex domain for both the Gaussian beam and the Laguerre polynomials, unlike in Equation (8), in which the argument shift into the complex plane takes place only for the Laguerre polynomial.

Using gHG beams, it is possible to create elliptical vortex HG beams different from those discussed in Ref. [10]. As a starting point, we use the summation formula of Hermite polynomials [47]:

$$\sum_{k=0}^n \binom{n}{k} t^k H_{n-k}(x) H_k(y) = (1+t^2)^{n/2} H_n\left(\frac{x+ty}{\sqrt{1+t^2}}\right). \tag{10}$$

Using Equations (5) and (10) for the superposition of gHG beams, the elliptical vortex HG beams can be derived in the following form:

$$\begin{aligned}
 \sum_{k=0}^n \binom{n}{k} t^k \text{gHG}_{n-k,k}(x, y, z|a, b) &= \frac{1}{q} \exp\left(-\frac{x^2+y^2}{w_0^2 q}\right) \\
 &\times \left(\frac{(1+t^2)(1-Tq)}{q}\right)^{n/2} H_n\left(\frac{x+ty}{w_0\sqrt{(1+t^2)q(1-Tq)}}\right),
 \end{aligned} \tag{11}$$

where  $T = (a + bt^2)/(1 + t^2)$ .

Substituting  $t = i\alpha$  with a real  $\alpha$  into (11), we obtain an elliptical optical vortex  $x + i\alpha y$  on the right-hand side in the argument of the Hermite polynomial. Hence, near every real null of the Hermite polynomial, which are found on the horizontal axis ( $a$  and  $b$  are real parameters), there is an optical vortex with a topological charge of  $+1$  ( $\alpha > 0$ ) or  $-1$  ( $\alpha < 0$ ). The modulus of the total topological charge of beam (11) equals  $n$ . At  $\alpha = \pm 1$ , the vortex Hermite beam in (11) is converted into a single-ring LG beam.

#### 4. Non-Orthogonality and Power of gLG Beams

With the parameter  $a$  being complex, the LG beams in (6) are not mutually orthogonal. Considering that the dot product of two solutions of a paraxial equation remains unchanged at any  $z$ , the non-orthogonality of the generalized LG beams can be proven in the source

plane (at the Gaussian beam waist). Actually, it can be shown that, in the source plane, the dot product of two generalized LG beams of (6) is given by

$$\int_0^\infty \int_0^{2\pi} \text{gLG}_{p,\ell}^*(r, \varphi, z|a) \text{gLG}_{n,m}(r, \varphi, z|a) r dr d\varphi = \frac{\pi\omega_0^2}{2} \cdot \frac{(n+m)!}{2^{p+n+m}n!} \delta_{\ell,m} \times \sum_{k=0}^{\min(n,p)} \binom{n}{k} \binom{p+n+m-k}{p-k} (1-2a^*)^{p-k} (1-2a)^{n-k} (4\text{Re}a - 4|a|^2)^k, \tag{12}$$

where  $\delta_{\ell,m}$  is the Kronecker symbol and  $(p, l)$  and  $(n, m)$  are the beams orders. In Equation (12), the generalized LG beams are seen to be orthogonal with respect to the azimuthal index, because at  $m \neq \ell$ , the right-hand side of (12) equals zero. Meanwhile, at different-valued radial indices,  $n \neq p$ , the right-hand side of (12), is non-zero. The only exception is  $a = \frac{1}{2}$  when the gLG beams are reduced to LG beams, becoming orthogonal with respect to both radial and azimuthal indices. Notably, from (12) follows an expression for the power  $W$  of a gLG beam:

$$W = \int_0^\infty \int_0^{2\pi} |\text{gLG}_{n,m}(r, \varphi, z|a)|^2 r dr d\varphi = \frac{\pi\omega_0^2}{2} \cdot \frac{(n+m)!}{2^{2n+m}n!} \times \sum_{k=0}^n \binom{n}{k} \binom{2n+m-k}{n-k} |1-2a|^{2n-2k} (4\text{Re}a - 4|a|^2)^k. \tag{13}$$

At  $a = \frac{1}{2}$ , Equation (13) can be seen to describe the power of standard LG beams:

$$W_{a=1/2} = 2^{2n} \int_0^\infty \int_0^{2\pi} \left| \text{gLG}_{n,m}(r, \varphi \left| \frac{1}{2} \right. \right) \right|^2 r dr d\varphi = \frac{\pi\omega_0^2(n+m)!}{2^{m+1}n!}. \tag{14}$$

### 5. Topological Charge of gLG Beams and Their Anomalous Rotation upon Propagation

Following M. V. Berry [49], we define the topological charge of an arbitrary light field by the formula

$$\text{TC} = \frac{1}{2\pi} \lim_{r \rightarrow \infty} \int_0^{2\pi} \arg E(r, \varphi) d\varphi \tag{15}$$

where  $E(r, \varphi)$  is the complex amplitude in the transverse plane and  $(r, \varphi)$  are polar coordinates in this plane.

The superposition (8) is described by a Laguerre polynomial of the  $n$ -th degree. Thus, at  $r \rightarrow \infty$ , it is mostly determined by its highest-degree term, and we can suppose that the right part of Equation (8) reads as

$$\text{gLG}_{n,m}(r, z|a, t \ll r) = \frac{1}{n!q} \exp\left(-\frac{r^2}{\omega_0^2 q}\right) \left(\frac{1-aq}{q}\right)^n \left(\frac{re^{i\varphi}}{\omega_0 q}\right)^m \left(\frac{-r^2}{\omega_0^2 q(1-aq)}\right)^n. \tag{16}$$

As seen in Equation (16), the TC of the whole superposition is thus equal to  $m$ , i.e., equal to the maximal TC in the superposition of the generalized LG beams. The generalized LG beams from Equation (6) have the same topological charge as of the conventional LG beams from Equation (2). In the next section, the simulation confirms this.

It can be seen in Equation (8) that if  $m > 0$ , then, upon propagation in free space, the transverse shape of the light beam should be rotated counterclockwise, as typically happens for most light beams.

However, the asymmetry of the intensity distribution is only affected by the Laguerre polynomial, since the absolute values of all other multipliers in Equation (8) are rotationally

symmetric. For simplicity, we consider a simple case,  $a = \frac{1}{2}$ , since the denominator of the argument of the Laguerre polynomial becomes real-valued. The argument  $\xi$  is thus equal to

$$\xi = 2 \frac{r^2 - tw(z)re^{i\varphi+i\gamma}}{w^2(z)} \tag{17}$$

where  $\gamma = \arctan(z/z_0)$  is the Gouy phase and where  $w(z) = w_0 |q(z)|$ . Equation (17) can be rewritten in the Cartesian coordinates:

$$\begin{aligned} \xi &= 2 \frac{x^2+y^2}{w^2(z)} - 2t \frac{x+iy}{w(z)} e^{i\gamma} \\ &= 2 \left( \frac{x}{w(z)} - \frac{t \cos \gamma}{2} \right)^2 + 2 \left( \frac{y}{w(z)} + \frac{t \sin \gamma}{2} \right)^2 - \frac{t^2}{2} - 2it \frac{y \cos \gamma + x \sin \gamma}{w(z)}. \end{aligned} \tag{18}$$

We see that the real part of the argument is, up to the constant  $-t^2/2$ , the distance from the point  $(x,y)$  to the point with coordinates

$$x_c = \frac{t}{2}w(z) \cos \gamma, \quad y_c = -\frac{t}{2}w(z) \sin \gamma. \tag{19}$$

To determine the transformation of the beam transverse shape on propagation, we should choose some characteristic points whose evolution we are able to trace. Equation (18) indicates that we can choose zero-intensity points. Since all the roots of the Laguerre polynomials are real [50],  $\text{Im } \xi = 0$  in these points. Actually, these points reside on the intersections of several concentric light rings (the roots of the Laguerre polynomial) with the center given by Equation (19), and of a straight line,  $y \cos \gamma + x \sin \gamma = 0$ . In the initial plane ( $z = 0$ ), the Gouy phase shift is zero ( $\gamma = 0$ ) and, thus,  $\xi$  is real at  $y = 0$ . The ring center is in the point  $(t/2, 0)$ . Thus, if  $t > 0$ , the considered zero-intensity points are to the right of the origin (Figure 1a). Then, after propagation over some distance  $z$ , the rings center moves to the point given by Equation (19), i.e., it is rotated clockwise by the angle  $-\gamma$  with respect to the origin. The value  $\xi$  is real at  $y = -x \tan \gamma = -xz/z_0$ , i.e., the straight line with real values  $\xi$  is also rotated clockwise by the angle  $\gamma$  (Figure 1b). In the far field,  $z \gg z_0$  and  $\gamma = \pi/2$ , the ring center is in the point  $(0, -t/2)$  and  $\xi$  is real at  $x = 0$  (Figure 1c).

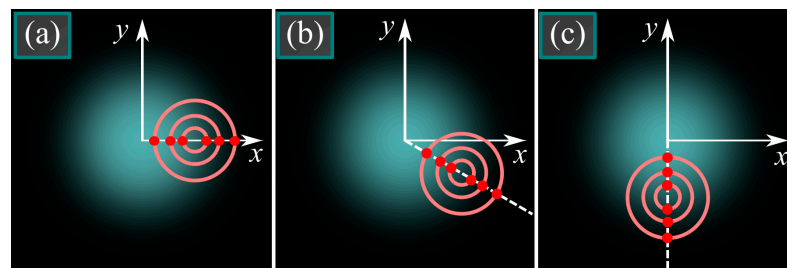


**Figure 1.** Schematic evolution of the asymmetric generalized Laguerre–Gaussian beam from Equation (8) shown as positions of zero-intensity points: in the initial plane (a), after propagation over some distance (b) and in the far field (c). Blue color denotes the rotationally symmetric part of the beam (Gaussian envelope with an optical vortex), whereas pink rings denote the rings where the Laguerre polynomial is zero (if the imaginary part of its argument is neglected). Red dots thus denote the points where the beam intensity is zero.

Thus, beam (8), consisting of the LG beams with positive topological charges  $m + s$ , is nevertheless rotated clockwise upon propagation. Spiral beams with this anomalous rotation have been investigated in [51], but beams (8) are different since  $2(n - k) + |m + k| + \theta(m + k)$  is not a constant at  $\theta = -1$  and depends on  $k$ .

### 6. Numerical Modeling of gLG Beams

In this section, we present the results of the computation of the asymmetric gLG beams. All the data were obtained in two ways: (1) using the numerical Fresnel transform,

implemented as a convolution by adopting the fast Fourier transform, and (2) using the theoretical Equation (8). In both cases, the intensity patterns are visually indistinguishable, while the phase patterns are only different in low-intensity areas. This confirms the correctness of Equation (8) for the complex amplitudes in space propagation.

Intensity and phase distributions of the symmetric and asymmetric gLG beams for some transverse planes are shown in Figure 2.

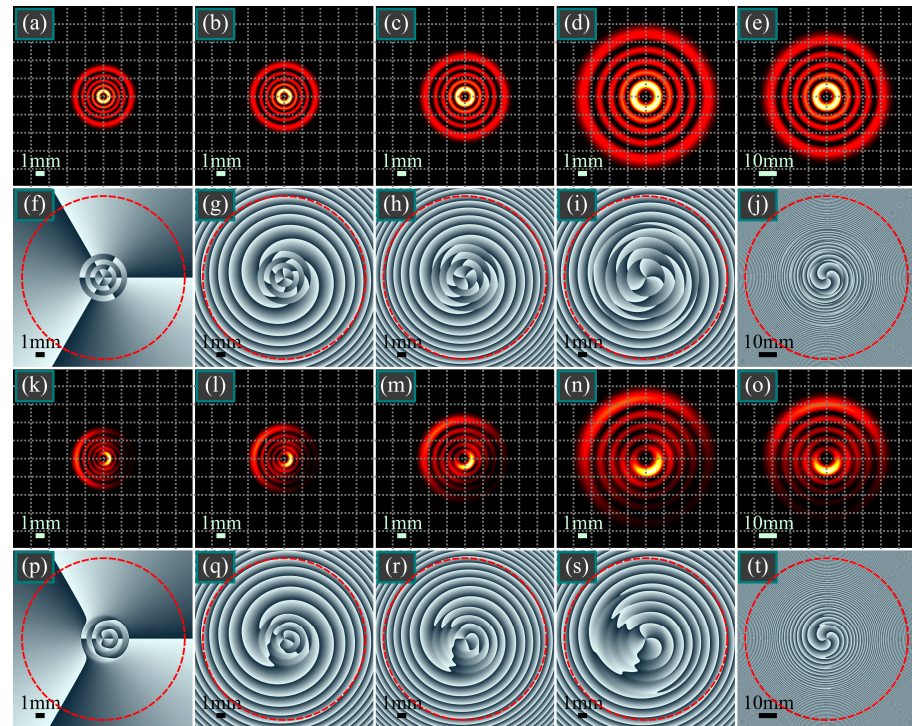


**Figure 2.** Intensity (a–e,k–o) and phase (f–j,p–t) distributions of the asymmetric gLG beams, regarding Equation (8), in some transverse planes for the following computation parameters: wavelength:  $\lambda = 532$  nm; Gaussian beam waist radius:  $w_0 = 1$  mm; radial index of the gLG beam:  $n = 4$ ; azimuthal index (topological charge):  $m = 3$ ; scaling factor:  $a = 1/2$ ; asymmetry parameter:  $t = 0$  (a–j) and  $t = 0.25$  (k–t); propagation distances:  $z = 0$  (a,f,k,p),  $z = z_0/2$  (b,g,l,q),  $z = z_0$  (c,h,m,r),  $z = 2z_0$  (d,i,n,s) and  $z = 10z_0$  (e,j,o,t). Dashed circles on the phase distributions bound the disks for the TC computation. All frames are shown in the square  $[-5c, 5c] \times [-5c, 5c]$ , where  $c = 2$  mm (a–d,f–i,k–n,p–s) and  $c = 10$  mm (e,j,o,t) are the sizes of the grid cell.

As seen in Figure 2, if  $a = 1/2$  and  $t = 0$ , the asymmetric gLG beam reduces to the conventional shape-invariant LG beam. When  $t = 0.25$ , the beam becomes asymmetric and, in agreement with the theory above, rotates clockwise upon propagation in free space. For each plane, we compute the TC value. The results are 3.0000 (Figure 2p), 2.9981 (Figure 2q), 2.9971 (Figure 2r), 2.9982 (Figure 2s) and 2.9295 (Figure 2t), i.e., the theoretical value of  $TC = 3$  is confirmed.

Now, let us consider what happens when the asymmetry parameter is further increased. Figure 3 illustrates the intensity and phase distributions of the symmetric and asymmetric gLG beams, regarding Equation (8), in some transverse planes when  $t = 1$  and  $t = 2$ .

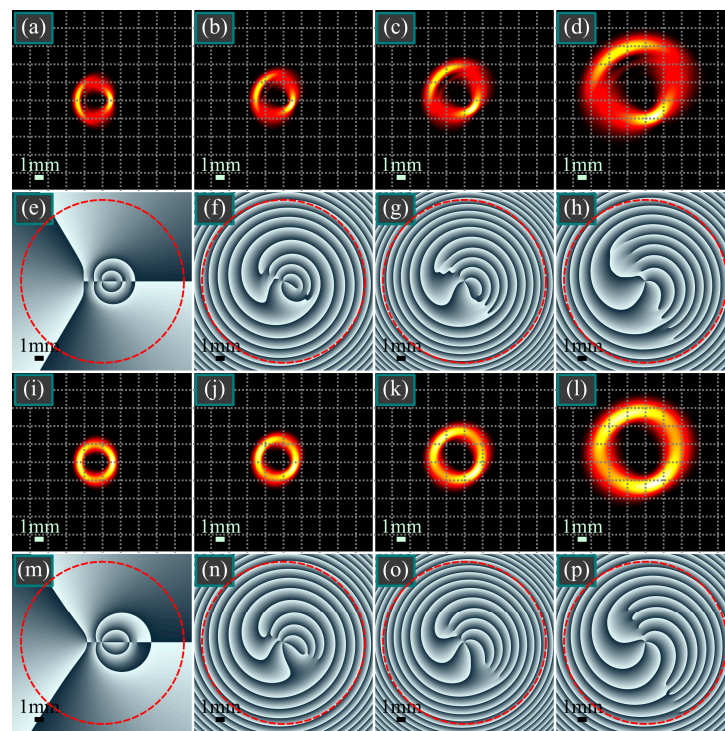


**Figure 3.** The same as Figure 2, but for  $t = 1$  (a–h) and  $t = 2$  (i–p).

According to Figure 3, when the asymmetry parameter is increased, only the central and the outermost rings become bright, while the other rings become pale. It can also be seen that the intensity trends towards a single ring shape (Figure 3i–l). This is predictable, since when  $t$  in Equation (8) grows, the most significant weight in this superposition is of the last LG beam, i.e., the beam with  $k = n$ . This is an exactly single-ringed LG beam (with the azimuthal index of  $m + n$ ).

The computed TC values in each plane are as follows: 3.0000 (Figure 3e), 2.9982 (Figure 3f), 2.9972 (Figure 3g), 2.9985 (Figure 3h), 3.0000 (Figure 3m), 2.9982 (Figure 3n), 2.9972 (Figure 3o) and 2.9988 (Figure 3p), i.e., the theoretical value of  $TC = 3$  is confirmed.

When the asymmetry parameter  $t$  becomes large enough, the single-ringed LG beam completely dominates in the superposition and the intensity distribution looks like a homogeneous ring (Figure 4). Then, looking at Equation (8), it may seem that this domination leads to the change of the TC to  $m + n$ . However, Figure 4 demonstrates that the TC remains equal to  $m$ , since there are additional  $n$  peripheral optical vortices of the charge  $-1$  (insets in Figure 4i–l). For instance, when the TC is computed over a disk of radius 9 mm (circles in Figure 4e–h), the obtained values are 7.0017 (Figure 4e), 6.9980 (Figure 4f), 6.9946 (Figure 4g) and 6.9968 (Figure 4h). When the disk radius for computation has been doubled (Figure 4i–k) or tripled (Figure 4l), the obtained values became 3.0000 (Figure 4i), 2.9704 (Figure 4j), 2.9534 (Figure 4k) and 2.9625 (Figure 4l).

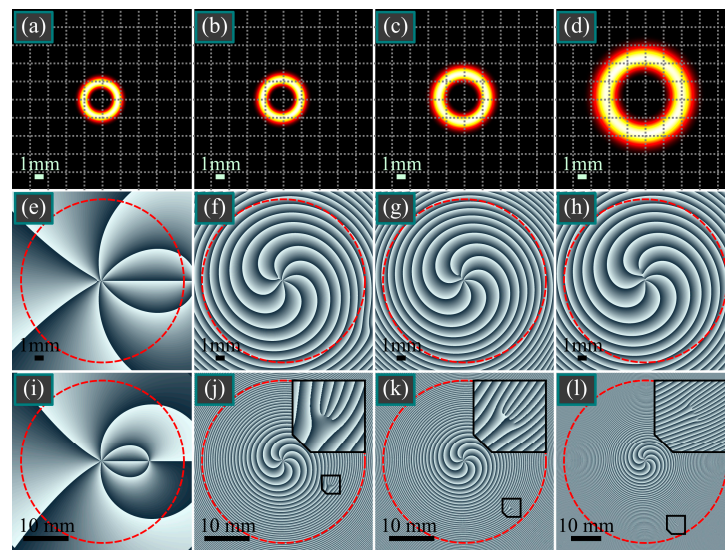


**Figure 4.** Intensity (a–d) and phase (e–l) distributions of the asymmetric gLG beams, regarding Equation (8), in some transverse planes for the following computation parameters: wavelength:  $\lambda = 532$  nm; Gaussian beam waist radius:  $w_0 = 1$  mm; radial index:  $n = 4$ ; azimuthal index (topological charge):  $m = 3$  of the LG beam; scaling factor:  $a = 1/2$ ; asymmetric parameter:  $t = 10$ ; propagation distances:  $z = 0$  (a,e,i),  $z = z_0/2$  (b,f,j),  $z = z_0$  (c,g,k) and  $z = 2z_0$  (d,h,l). Dashed circles on the phase distributions bound the disks of the TC computation. Phase distributions in the bottom row are the same as above but the area is enlarged. The insets (j–l) show the 4-fold zoomed regions with additional vortices.

### 7. Numerical Modeling of gHG Beams

First, we compare gHG beams with standard and elegant HG beams. Figure 5 depicts the intensity and phase distributions of HG beams  $n = m = 5$ , as can be seen in Equation (1), whose shape is conserved upon propagation in both transverse directions (a–h); of eHG beams  $n = m = 5$ , as can be seen in Equation (3), whose shape is changed (i–p); and of gHG beams  $n = m = 5$ , as can be seen in Equation (5), whose shape is conserved in one transverse direction and is changed in another direction (q–x).

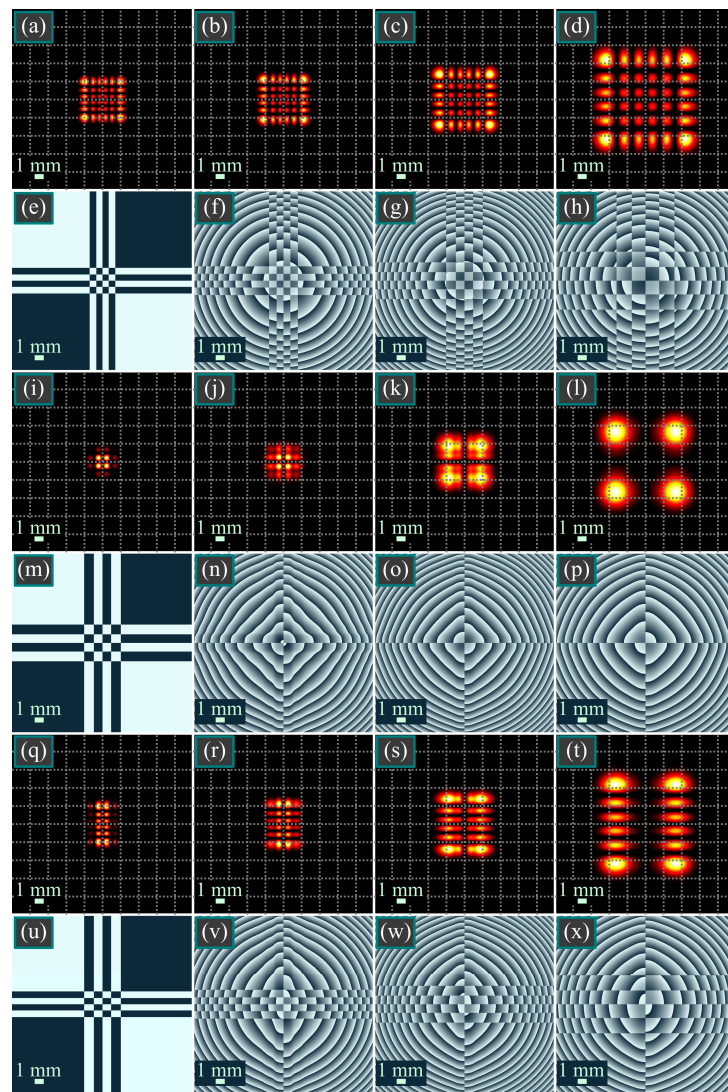


**Figure 5.** Intensity (a–d,i–l,q–t) and phase (e–h,m–p,u–x) distributions of gHG beams, regarding Equation (5), (i.e., without the asymmetry) in some transverse planes for the following computation parameters: wavelength:  $\lambda = 532$  nm; Gaussian beam waist radius:  $w_0 = 1$  mm; orders of the HG beams:  $m = 5$  and  $n = 5$ ; scaling factors:  $a = 1/2$  and  $b = 1/2$  (a–h),  $a = 0$  and  $b = 0$  (i–p),  $a = 0$  and  $b = 1/2$  (q–x); propagation distances:  $z = 0$  (a,e,i,m),  $z = z_0/2$  (b,f,j,n),  $z = z_0$  (c,g,k,o) and  $z = 2z_0$  (d,h,l,p). All frames are shown in the square  $[-5c, 5c] \times [-5c, 5c]$ , where  $c = 2$  mm is the size of the grid cell.

As can be seen in Figure 5, all three beams are symmetrical with respect to the Cartesian axes.

Figure 6 illustrates the asymmetric generalized gHG beams with  $n = m = 5$  that have two real-valued parameters:  $t$  and  $\tau$ . Since the beam is different in different transverse directions along the axes  $x$  and  $y$ , for the changes to be more visible, we apply a different asymmetry along these axes.

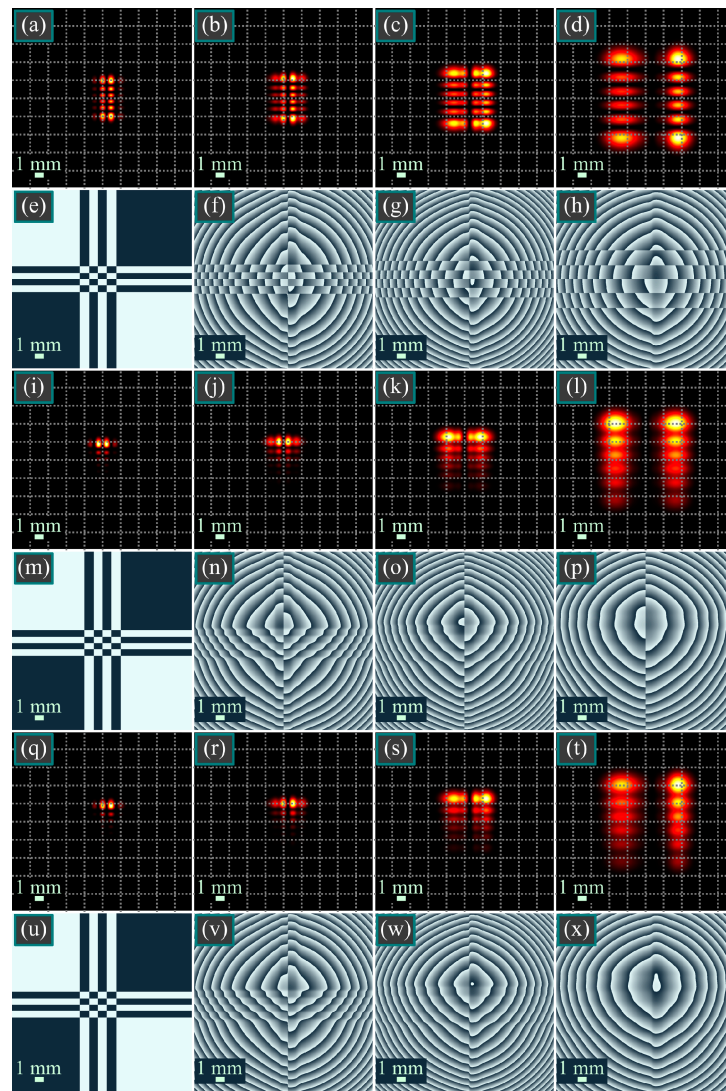
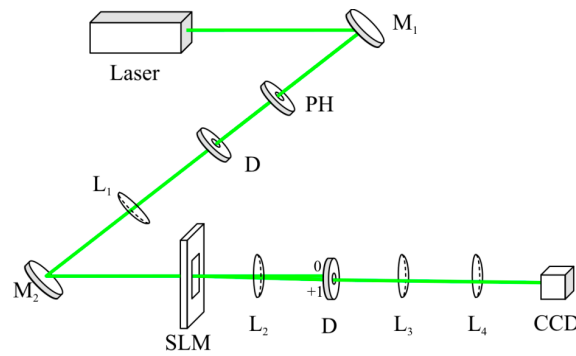


**Figure 6.** Intensity (a–d,i–l,q–t) and phase (e–h,m–p,u–x) distributions of asymmetric gHG beams, regarding Equation (9), in some transverse planes for the following computation parameters: wavelength:  $\lambda = 532$  nm; Gaussian beam waist radius:  $w_0 = 1$  mm; orders of the gHG beams:  $m = 5$  and  $n = 5$ ; scaling factors:  $a = 0$  and  $b = 1/2$ ; asymmetry parameters:  $t = 0$  and  $\tau = 1/2$  (a–h),  $t = 1/4$  and  $\tau = 0$  (i–p) and  $t = 1/4$  and  $\tau = 1/2$  (q–x); propagation distances:  $z = 0$  (a,e,i,m),  $z = z_0/2$  (b,f,j,n),  $z = z_0$  (c,g,k,o) and  $z = 2z_0$  (d,h,l,p). All frames are shown in the square  $[-5c, 5c] \times [-5c, 5c]$ , where  $c = 2$  mm is the size of the grid cell.

As expected, the nonzero parameter  $\tau$  breaks the intensity asymmetry with respect to the axis  $y$  (Figure 6a–h). Similarly, the nonzero parameter  $t$  breaks the intensity asymmetry with respect to the axis  $x$  (Figure 6i–p). When both the parameters  $t$  and  $\tau$  are nonzero, both asymmetries are broken (Figure 6q–x). Thus, setting the parameters  $t$  and  $\tau$  allows us to change the intensity shape in the beam cross-section.

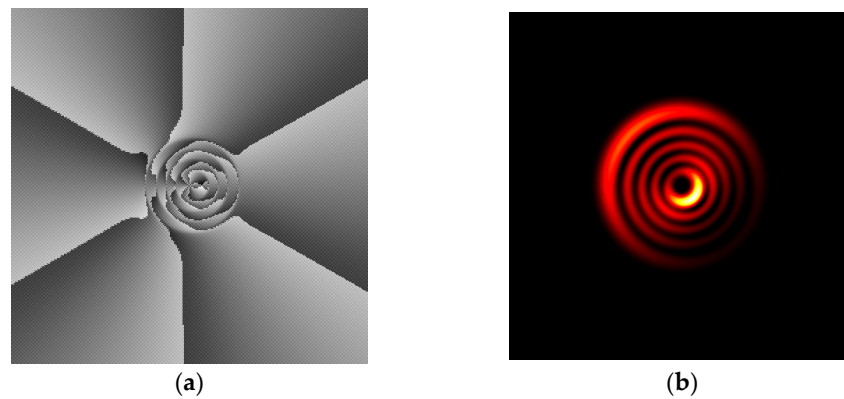
### 8. Experiment

Figure 7 illustrates the optical setup for the experiment. A light beam from the laser impinges onto the SLM, after which three diffraction orders occur. The diaphragm D transmits the working first diffraction order, whereas the spherical lens  $L_4$  ( $f = 250$  mm) focuses it. The CCD matrix registers several intensity distributions near the focus.



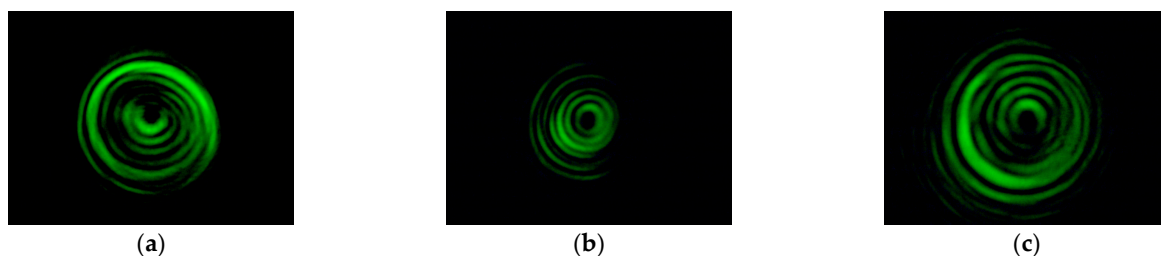
**Figure 7.** Experimental setup. Laser–MGL-F-532-700 ( $\lambda = 532 \text{ nm}$ ),  $M_1$ ,  $M_2$ –mirrors, PH–pinhole,  $L_1$ – $L_4$ –spherical lenses ( $f_1 = 750 \text{ mm}$ ,  $f_2 = 150 \text{ mm}$ ,  $f_3 = 100 \text{ mm}$ ,  $f_4 = 250 \text{ mm}$ ), D–diaphragm, SLM–spatial light modulator (Holoeye LC 2012), CCD–CCD camera (UCMOS10000KPA).

Figure 8a depicts the phase distribution generated in the SLM display. The phase from Figure 8a encodes the amplitude and phase of the asymmetric generalized LG beam from Equation (8) with the same parameters as in Figure 2m. The computed intensity distribution generated by the phase is shown in Figure 8b.



**Figure 8.** Encoded phase (a) intended for generating an asymmetric generalized LG beam from Equation (8) with the same parameters as in Figure 2m:  $n = 4$ ,  $m = 3$ ,  $a = 1/2$ ,  $t = 0.25$  (b).

Figure 9 depicts the intensity distributions at different distances before and after the focus, registered by the CCD-matrix in the optical setup from Figure 7 with using the phase from Figure 8a in the SLM.



**Figure 9.** Intensity distributions registered by the CCD-camera in the setup from Figure 7 at a distance of 2 mm before the focus of the lens  $L_4$  (a), near the focus (b) and at a distance of 2 mm after the focus (c). The frame sizes are  $(1 \times 0.75) \text{ mm}$ .

As can be seen in Figure 9, the experimental intensity patterns are qualitatively consistent with the computed pattern shown in Figure 8b. It can be seen that the energy goes mostly into the inner and outer light rings. Both these rings have the shape of a crescent and rotate on propagation.

## 9. Conclusions

Summing up, we have derived novel exact solutions of the paraxial propagation equation. Relationships have also been deduced for the complex amplitudes that describe the propagation of asymmetric gHG and gLG beams in (8) and (9). The derived relationships contain parameter sets, with the amplitude of an asymmetric gLG beam being described by two complex parameters, namely, the scale parameter and the asymmetry degree parameter. The amplitude of an asymmetric gHG beam contains four parameters, divided into pairs for each Cartesian axis. With the original generalized elegant HG (5) and LG (6) beams not retaining their intensity pattern upon free-space propagation, the derivative generalized asymmetric HG and LG beams also do not retain their intensity pattern in the course of their propagation evolution. The generalized LG beams of Equation (9) are not orthogonal with regard to the radial indices, meaning that the asymmetric LG beams of Equation (10) are also non-orthogonal with regard to the radial indices. For the generalized LG beams, we have proved that their topological charge is independent of the asymmetry and equals the upper index of the Laguerre polynomial. We have also found that the asymmetric LG beam is anomalously rotated upon propagation in free space, i.e., it is rotated clockwise when the vortex factor has a positive topological charge.

Another finding of this work is the relationship of the complex amplitude of a family of generalized vortex HG beams in Equation (11), which is characterized by three parameters, with two parameters defining the beam scale and a complex parameter defining the asymmetry degree of elliptical optical vortices of unit topological charge, with the vortices centered at the zeros of a Hermite polynomial.

The proposed generalized asymmetrical laser beams can be realized using an SLM, with the adoption of some techniques for the encoding and amplitude-phase function into a phase-only one [52,53], utilized for data transmission through atmospheric turbulence. The scale parameters and the parameter controlling the asymmetry degree offer additional degrees of freedom [54] enabling the creation of a beam least prone to distortion due to turbulence. We note that attractive beams for optical communications are non-diffractive beams such as Bessel beams [55] or Airy beams [56]. However, Laguerre and Hermite Gaussian beams are also used for these tasks [57].

The asymmetric generalized LG beams from Equation (8) can also be used for trapping and rotating microparticles along a light arc [46] or for trapping and shifting biological cell-like microobjects without damaging them [28]. Asymmetric generalized HG beams from Equation (9) constitute a four-parametric family. Changing these parameters allows us to control the intensity distribution in the beam cross-section. Such beams can be used for accelerating microparticles [58]. Asymmetric generalized LG beams from Equation (8) rotate upon propagation (Figures 2 and 3). This property can be used in optical metrology [59] for measuring the longitudinal beam shift by measuring the rotation angle of the asymmetric intensity pattern in the beam cross-section [60].

**Author Contributions:** Conceptualization, E.G.A.; methodology, E.G.A. and V.V.K.; software, A.A.K.; validation, V.V.K.; formal analysis, E.G.A.; investigation, E.G.A., V.V.K., A.A.K. and S.S.S.; resources, V.V.K.; data curation, V.V.K.; writing—original draft preparation, V.V.K.; writing—review and editing, E.G.A. and V.V.K.; visualization, A.A.K.; supervision, V.V.K.; project administration, V.V.K.; funding acquisition, V.V.K. and A.A.K. All authors have read and agreed to the published version of the manuscript.

**Funding:** The work was partly funded by the Russian Science Foundation under grant No. 22-12-00137 (Theoretical background). This work was also performed within the State assignment of Federal Scientific Research Center “Crystallography and Photonics” of Russian Academy of Sciences (in parts about numerical modeling).

**Institutional Review Board Statement:** Not applicable.

**Informed Consent Statement:** Not applicable.

**Data Availability Statement:** Not applicable.

**Conflicts of Interest:** The authors declare no conflict of interest. The funders had no role in the design of the study; in the collection, analyses, or interpretation of data; in the writing of the manuscript; or in the decision to publish the results.

## References

1. Kogelnik, H.; Li, T. Laser beams and resonators. *Appl. Opt.* **1966**, *5*, 1550–1567. [[CrossRef](#)] [[PubMed](#)]
2. Siegman, A.E. Hermite-Gaussian functions of complex argument as optical beam eigenfunction. *J. Opt. Soc. Am.* **1973**, *63*, 1093–1094. [[CrossRef](#)]
3. Pratesi, R.; Ronchi, L. Generalized Gaussian beams in free space. *J. Opt. Soc. Am.* **1977**, *67*, 1274–1276. [[CrossRef](#)]
4. Zauderer, E. Complex argument Hermite-Gaussian and Laguerre-Gaussian beams. *J. Opt. Soc. Am. A* **1986**, *3*, 465–469. [[CrossRef](#)]
5. Wünsche, A. Generalized Gaussian beam solutions of paraxial optics and their connection to a hidden symmetry. *J. Opt. Soc. Am. A* **1989**, *6*, 1320–1329. [[CrossRef](#)]
6. Kotlyar, V.V.; Kovalev, A.A. Hermite-Gaussian modal laser beams with orbital angular momentum. *J. Opt. Soc. Am. A* **2014**, *31*, 274–282. [[CrossRef](#)]
7. Wang, Y.; Chen, Y.; Zhang, Y.; Chen, H.; Yu, S. Generalised Hermite-Gaussian beams and mode transformations. *J. Opt.* **2016**, *18*, 055001. [[CrossRef](#)]
8. Abramochkin, E.G.; Volostnikov, V.G. Generalized Gaussian beams. *J. Opt. A Pure Appl. Opt.* **2004**, *6*, S157–S161. [[CrossRef](#)]
9. Abramochkin, E.G.; Volostnikov, V.G. Beam transformations and nontransformed beams. *Opt. Commun.* **1991**, *83*, 123–135. [[CrossRef](#)]
10. Kotlyar, V.V.; Kovalev, A.A.; Porfirev, A.P. Vortex Hermite-Gaussian laser beams. *Opt. Lett.* **2015**, *40*, 701–704. [[CrossRef](#)]
11. Mei, Z.; Zhao, D.; Gu, J.; Mao, H. Approximate analytical expressions of Laguerre-Gaussian beams passing through a paraxial optical system with an annular aperture. *Optik* **2004**, *115*, 311–316. [[CrossRef](#)]
12. Arlt, J.; Kuhn, R.; Dholakia, K. Spatial transformation of Laguerre-Gaussian laser modes. *J. Mod. Opt.* **2001**, *48*, 783–787. [[CrossRef](#)]
13. Jarutis, V.; Paškauskas, R.; Stabinis, A. Focusing of Laguerre-Gaussian beams by axicon. *Opt. Commun.* **2000**, *184*, 105–112. [[CrossRef](#)]
14. Simon, R.; Agarwal, G.S. Wigner representation of Laguerre-Gaussian beams. *Opt. Lett.* **2000**, *25*, 1313–1315. [[CrossRef](#)] [[PubMed](#)]
15. Kim, H.C.; Lee, Y.H. Hermite-Gaussian and Laguerre-Gaussian beams beyond the paraxial approximation. *Opt. Commun.* **1999**, *169*, 9–16. [[CrossRef](#)]
16. Hasegawa, T.; Shimizu, T. Frequency-doubled Hermite-Gaussian beam and the mode conversion to the Laguerre-Gaussian beam. *Opt. Commun.* **1999**, *160*, 103–108. [[CrossRef](#)]
17. Kovalev, A.A.; Kotlyar, V.V.; Porfirev, A.P. Asymmetric Laguerre-Gaussian beams. *Phys. Rev. A* **2016**, *93*, 063858. [[CrossRef](#)]
18. Hsieh, Y.H.; Lai, Y.H.; Hsieh, M.X.; Huang, K.F.; Chen, Y.F. Generating high-power asymmetrical Laguerre-Gaussian modes and exploring topological charges distribution. *Opt. Express* **2018**, *26*, 31738–31749. [[CrossRef](#)]
19. Ghaderi Goran Abad, M.; Mahmoudi, M. Laguerre-Gaussian modes generated vector beam via nonlinear magneto-optical rotation. *Sci. Rep.* **2021**, *11*, 5972. [[CrossRef](#)]
20. Yang, Y.; Li, Y.; Wang, C. Generation and expansion of Laguerre-Gaussian beams. *J. Opt.* **2022**, *51*, 910–926. [[CrossRef](#)]
21. Matsumoto, N.; Ando, T.; Inoue, T.; Ohtake, Y.; Fukuchi, N.; Hara, T. Generation of high-quality higher-order Laguerre-Gaussian beams using liquid-crystal-on-silicon spatial light modulators. *J. Opt. Soc. Am. A* **2008**, *25*, 1642–1651. [[CrossRef](#)] [[PubMed](#)]
22. Volyar, A.; Abramochkin, E.; Akimova, Y.; Bretsko, M. Control of the orbital angular momentum via radial numbers of structured Laguerre-Gaussian beams. *Opt. Lett.* **2022**, *47*, 2402–2405. [[CrossRef](#)]
23. Volyar, A.; Abramochkin, E.; Akimova, Y.; Bretsko, M. Astigmatic-Invariant Structured Singular Beams. *Photonics* **2022**, *9*, 842. [[CrossRef](#)]
24. Kotlyar, V.V.; Khonina, S.N.; Almazov, A.A.; Soifer, V.A.; Jefimovs, K.; Turunen, J. Elliptic Laguerre-Gaussian beams. *J. Opt. Soc. Am. A* **2006**, *23*, 43–56. [[CrossRef](#)] [[PubMed](#)]
25. Dwivedi, R.; Sharma, P.; Jaiswal, V.K.; Mehrotra, R. Elliptically squeezed axicon phase for detecting topological charge of vortex beam. *Opt. Commun.* **2021**, *485*, 126710. [[CrossRef](#)]
26. Kotlyar, V.V.; Kovalev, A.A.; Soifer, V.A. Asymmetric Bessel modes. *Opt. Lett.* **2014**, *39*, 2395–2398. [[CrossRef](#)]
27. Gong, L.; Qiu, X.Z.; Ren, Y.X.; Zhu, H.Q.; Liu, W.W.; Zhou, J.H.; Zhong, M.C.; Chu, X.X.; Li, Y.M. Observation of the asymmetric Bessel beams with arbitrary orientation using a digital micromirror device. *Opt. Express* **2014**, *22*, 26763–26776. [[CrossRef](#)]
28. Rykov, M.A.; Skidanov, R.V. Modifying the laser beam intensity distribution for obtaining improved strength characteristics of an optical trap. *Appl. Opt.* **2014**, *53*, 156–164. [[CrossRef](#)]
29. Beijersbergen, M.W.; Allen, L.; van der Veen, H.E.L.O.; Woerdman, J.P. Astigmatic laser mode converters and transfer of orbital angular momentum. *Opt. Commun.* **1993**, *96*, 123–132. [[CrossRef](#)]
30. Heckenberg, N.R.; McDuff, R.; Smith, C.P.; White, A.G. Generation of optical phase singularities by computer-generated holograms. *Opt. Lett.* **1992**, *17*, 3. [[CrossRef](#)]
31. Dennis, M.R.; O'Holleran, K.; Padgett, M.J. Chapter 5 Singular Optics: Optical Vortices and Polarization Singularities. *Prog. Opt.* **2009**, *53*, 293–363. [[CrossRef](#)]
32. Kim, G.H.; Jeon, J.H.; Ko, K.H.; Lee, J.H.; Chang, J.S. Optical vortices produced with a nonspiral phase plate. *Appl. Opt.* **1997**, *36*, 8614–8621. [[CrossRef](#)] [[PubMed](#)]

33. Marrucci, L.; Manzo, C.; Paparo, D. Optical spin-to-orbital angular momentum conversion in inhomogeneous anisotropic media. *Phys. Rev. Lett.* **2006**, *96*, 163905. [[CrossRef](#)] [[PubMed](#)]
34. Senatsky, Y.; Bisson, J.F.; Shelobolin, A.; Shirekawa, A.; Ueda, K. Circular modes selection in Yb:YAG laser using an intracavity lens with spherical aberration. *Laser Phys.* **2009**, *19*, 911–918. [[CrossRef](#)]
35. Thirugnanasambandam, M.P.; Senatsky, Y.; Ueda, K. Generation of very-high order Laguerre-Gaussian modes in Yb:YAG ceramic laser. *Laser Phys. Lett.* **2010**, *7*, 637–643. [[CrossRef](#)]
36. Tan, S.; Zhou, C.; Shirakakwa, A.; Ueda, K.; Li, J. Vortex Ti:Sapphire laser by using an intracavity spot-defect spatial filter. *Opt. Laser Technol.* **2017**, *96*, 76–80. [[CrossRef](#)]
37. Ngcobo, S.; Litvin, I.; Burger, L.; Forbes, A. A digital laser for on-demand laser modes. *Nat. Commun.* **2013**, *4*, 2289. [[CrossRef](#)]
38. Liu, S.S.; Chen, X.D.; Pu, J.X.; Lin, Z.L.; Chen, Z.Y. A V-folded digital laser for on-demand vortex beams by astigmatic transformation of Hermite-Gaussian modes. *Chinese Phys. Lett.* **2019**, *36*, 124203. [[CrossRef](#)]
39. Ito, A.; Kozawa, Y.; Sato, S. Generation of hollow scalar and vector beams using a spot-defect mirror. *J. Opt. Soc. Am. A.* **2010**, *27*, 2072–2077. [[CrossRef](#)]
40. Kano, K.; Kozawa, Y.; Sato, S. Generation of a Purely Single Transverse Mode Vortex Beam from a He-Ne Laser Cavity with a Spot-Defect Mirror. *Int. J. Opt.* **2012**, *2012*, 359141. [[CrossRef](#)]
41. Vyas, S.; Kozawa, Y.; Sato, S. Generation of a vector doughnut beam from an internal mirror He-Ne laser. *Opt. Lett.* **2014**, *39*, 2080–2082. [[CrossRef](#)] [[PubMed](#)]
42. Qiao, Z.; Xie, G.; Wu, Y.; Yuan, P.; Ma, J.; Qian, L.; Fan, D. Generating high-charge optical vortices directly from laser up to 288th order. *Laser Photon. Rev.* **2018**, *12*, 1800019. [[CrossRef](#)]
43. Uesugi, Y.; Sato, S.; Kozawa, Y. Direct generation of the lowest order vortex beam using a spot defect mirror in the ultraviolet region. *Opt. Lett.* **2020**, *45*, 2115–2118. [[CrossRef](#)] [[PubMed](#)]
44. Yu, L.; Zhang, Y.; Wang, J. Propagation of asymmetric Bessel mode in turbulent atmosphere. *IEEE Photonics J.* **2022**, *14*, 7354106. [[CrossRef](#)]
45. Watkins, R.J.; Dai, K.; White, G.; Li, W.; Miller, J.K.; Morgan, K.S.; Johnson, E.G. Experimental probing of turbulence using a continuous spectrum of asymmetric OAM beams. *Opt. Express* **2020**, *28*, 924–935. [[CrossRef](#)] [[PubMed](#)]
46. Kovalev, A.A.; Kotlyar, V.V.; Porfirev, A.P. Optical trapping and moving of microparticles by using asymmetrical Laguerre-Gaussian beams. *Opt. Lett.* **2016**, *41*, 2426–2429. [[CrossRef](#)]
47. Prudnikov, A.P.; Brychkov, Y.A.; Marichev, O.I. *Integrals and Series. Special Functions*; Gordon and Breach: New York, NY, USA, 1986.
48. Brychkov, Y.A. *Handbook of Special Functions: Derivatives, Integrals, Series and Other Formulas*; CRC Press: Boca Raton, FL, USA, 2008.
49. Berry, M.V. Optical vortices evolving from helicoidal integer and fractional phase steps. *J. Opt. A Pure Appl. Opt.* **2004**, *6*, 259. [[CrossRef](#)]
50. Abramowitz, M.; Stegun, I.A. *Handbook of Mathematical Functions*; Dover: New York, NY, USA, 1972.
51. Abramochkin, E.G.; Volostnikov, V.G. Spiral light beams. *Phys. Usp.* **2004**, *47*, 1177–1203. [[CrossRef](#)]
52. Mendoza-Yero, O.; Mínguez-Vega, G.; Lancis, J. Encoding complex fields by using a phase-only optical element. *Opt. Lett.* **2014**, *39*, 1740–1743. [[CrossRef](#)]
53. Goorden, S.; Bertolotti, J.; Mosk, A. Superpixel-based spatial amplitude and phase modulation using a digital micromirror device. *Opt. Express* **2014**, *22*, 17999–18009. [[CrossRef](#)]
54. Singh, S.K.; Adachi, Y.; Kinashi, K.; Tsutsumi, N.; Sakai, W.; Jackin, B.J. Tailoring Large Asymmetric Laguerre-Gaussian Beam Array Using Computer-Generated Holography. *Photonics* **2023**, *10*, 247. [[CrossRef](#)]
55. Durnin, J. Exact solutions for nondiffracting beams. I. The scalar theory. *J. Opt. Soc. Am. A* **1987**, *4*, 651–654. [[CrossRef](#)]
56. Siviloglou, G.A.; Broky, J.; Dogariu, A.; Christodoulides, D.N. Observation of Accelerating Airy Beams. *Phys. Rev. Lett.* **2007**, *99*, 213901. [[CrossRef](#)] [[PubMed](#)]
57. Cox, M.A.; Maqondo, L.; Kara, R.; Milione, G.; Cheng, L.; Forbes, A. The Resilience of Hermite- and Laguerre-Gaussian Modes in Turbulence. *J. Lightwave Technol.* **2019**, *37*, 3911–3917. [[CrossRef](#)]
58. Bochove, E.J.; Moore, G.T.; Scully, M.O. Acceleration of particles by an asymmetric Hermite-Gaussian laser beam. *Phys. Rev. A* **1992**, *46*, 6640–6653. [[CrossRef](#)]
59. Guo, M.; Le, W.; Wang, C.; Rui, G.; Zhu, Z.; He, J.; Gu, B. Generation, Topological Charge, and Orbital Angular Momentum of Off-Axis Double Vortex Beams. *Photonics* **2023**, *10*, 368. [[CrossRef](#)]
60. Pavani, S.R.P.; Piestun, R. High-efficiency rotating point spread functions. *Opt. Express* **2008**, *16*, 3484. [[CrossRef](#)]

**Disclaimer/Publisher’s Note:** The statements, opinions and data contained in all publications are solely those of the individual author(s) and contributor(s) and not of MDPI and/or the editor(s). MDPI and/or the editor(s) disclaim responsibility for any injury to people or property resulting from any ideas, methods, instructions or products referred to in the content.